Pulsed Laser Deposition of Photoresponsive Two-Dimensional GaSe Nanosheet Networks

Masoud Mahjouri-Samani, Ryan Gresback, Mengkun Tian, Kai Wang, Alexander A. Puretzky, Christopher M. Rouleau, Gyula Eres, Ilia N. Ivanov, Kai Xiao, Michael A. McGuire, Gerd Duscher, and David B. Geohegan*

Synthesis of functional metal chalcogenide (GaSe) nanosheet networks by stoichiometric transfer of laser-vaporized material from bulk GaSe targets is presented. Uniform coverage of interconnected, crystalline, and photoresponsive GaSe nanosheets in both in-plane and out-of-plane orientations are achieved under different ablation conditions. The propagation of the laser-vaporized material is characterized by in situ ICCD-imaging. High (1 Torr) Ar background gas pressure is found to be crucial for the stoichiometric growth of GaSe nanosheet networks. Individual 1–3 layer GaSe triangular nanosheets of ≈200 nm domain size are formed within 30 laser pulses, coalescing to form nanosheet networks in as few as 100 laser pulses. The thickness of the deposited networks increases linearly with pulse number, adding layers in a two-dimensional (2D) growth mode. GaSe nanosheet networks show p-type semiconducting characteristics with mobilities reaching as high as 0.1 $cm^2V^{-1}s^{-1}$. Spectrally-resolved photoresponsivities and external quantum efficiencies range from 0.4 AW^{-1} and 100% at 700 nm, to 1.4 AW^{-1} and 600% at 240 nm, respectively. Pulsed laser deposition under these conditions appears to provide a versatile and rapid approach to stoichiometrically transfer and deposit functional networks of 2D nanosheets with digital thickness control and uniformity for a variety of applications.

1. Introduction

The discovery of fascinating optical and electronic properties in atomically-thin two-dimensional (2D) graphene, with extremely high electron and hole mobilities (≈200 000 $cm^2V^{-1}s^{-1}$), has produced great interest in exploring and applying these properties in future optoelectronic devices.[1–4] However, lack of an electronic bandgap,[1] and therefore low on/off ratios in graphene-based electronics, has motivated researchers to explore single- and few-layer nanosheets of other 2D materials beyond graphene. Nanosheets of other layered materials, such as MoS_2, WS_2, GaS, $NbSe_2$, h-BN, Bi_2Te_3, etc., in single- and few-layer thicknesses are revealing extraordinary electrical and optical properties due to changes in the band structure that result from quantum confinement.[5–15] For instance, over the past few years a vast amount of research has been reported on the extraordinary optoelectronic properties of MoS_2 for both large-scale sheets and networks of small nanosheets.[16–18] Several methods have been explored to controllably produce crystalline single- or few-layer nanosheets for study on various substrates including chemical exfoliation,[5] atomic layer deposition,[6] mechanical cleavage,[8–11] chemical vapor deposition,[14] and vapor phase mass transport.[15] As in the case of graphene, synthesis and processing techniques to produce stoichiometric and crystalline nanosheet networks with high mobility and controllable layer thickness are highly desired.

Among transitional metal chalcogenides, gallium selenide (GaSe) is a typical example of a layered material made of covalently bonded sheets of Se-Ga-Ga-Se layers,[19] and is widely used in optics,[20] optoelectronics,[9,15,21] and terahertz applications.[22,23] GaSe has a D_{3h} symmetry with a lattice constant of 0.374 nm. GaSe is typically p-type semiconductor with an indirect bandgap of 2.11 eV that is only 25 meV lower than its direct bandgap. Recently, electrical transport and the photoresponse of exfoliated[9,10] and vapor phase[15] deposited GaSe has been reported showing their potential properties in optoelectronic devices.[9,10,15]

Here we report a laser-based approach for the deposition of GaSe nanosheet networks on insulating substrates with high spatial uniformity and thickness control by pulse number. The approach takes advantage of the spatial confinement of the ablation plume in relatively high background gas

Dr. M. Mahjouri-Samani, Dr. R. Gresback, Dr. K. Wang, Dr. A. A. Puretzky, Dr. C. M. Rouleau, Dr. I. N. Ivanov, Dr. K. Xiao, Dr. D. B. Geohegan
Center for Nanophase Materials Sciences
Oak Ridge National Laboratory
Oak Ridge, TN, USA
E-mail: mzs@ornl.gov
Dr. G. Eres, Dr. M. A. McGuire
Materials Science and Technology Division
Oak Ridge National Laboratory
Oak Ridge, TN, USA
M. Tian, Prof. G. Duscher
Dept. of Materials Science and Engineering
University of Tennessee
Knoxville, TN, USA

DOI: 10.1002/adfm.201401440

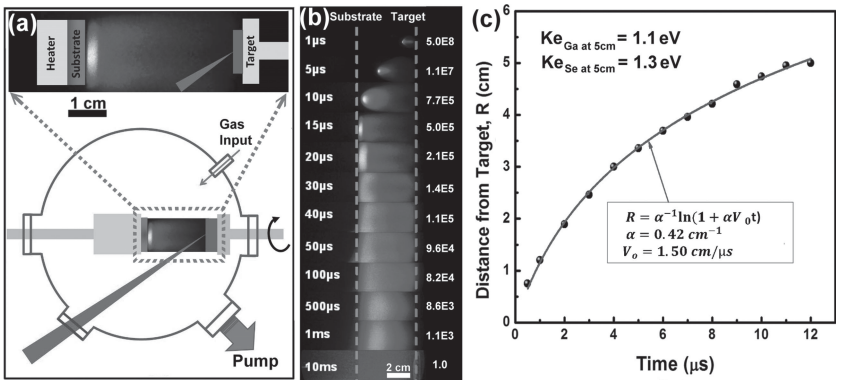

Figure 1. a) Schematic of the experimental setup. b) Time resolved imaging of visible plasma plume luminescence (numbers to the right of the plumes show the relative intensities) at the indicated times (numbers to the left) after laser ablation in 1Torr Ar and 600 °C substrate temperature. c) R-t plot of the plasma plume front (black dots) derived from the ICCD images. The curve fit (blue line) utilizes the phenomenological $a = -\alpha v^2$ drag model, where $v = \frac{v_0}{1+\alpha v_0 t}$; $R = \alpha^{-1}\ln(1+\alpha v_0 t)$.[24] The kinetic energies of the Ga and Se atoms at the surface of the substrate drops to 1.19 and 1.34eV, respectively.

pressures (≈1 Torr Ar) to achieve the stoichiometric transfer of the materials from the target and tune the kinetic energy of the precursor flux. Plume conditions were adjusted to provide sufficient instantaneous flux and kinetic energy for high nucleation densities of GaSe triangular nanosheet islands across the ≈1.5 cm^2 area of the substrate. With increasing pulse number, the ≈200 nm-sized triangular domains rapidly grew and coalesced to form interconnected networks. The crystalline GaSe networks show p-type semiconductor characteristics with high mobility (0.1 cm^{2}V^{-1}s^{-1}) and high photoresponsivity (0.4–1.4 AW^{-1}, from 700–240 nm).

2. Results and Discussion

Figure 1 shows a schematic illustration of the pulsed laser deposition setup and the propagation of the laser plume under optimal growth conditions. Typically, pulsed laser deposition (PLD) involves the generation of a highly forward-directed laser plasma consisting of high kinetic-energy ions and neutral atoms, followed by slower moving molecules and clusters.[24] In vacuum, the highly nonequilibrium PLD process can produce fast ions and neutrals with sufficiently high kinetic energies (>100 eV) to form ultrahard thin films, but more typically background gases are used to moderate kinetic energies to ≈1 eV for the growth of thin films or nanoparticles where the sticking, evaporation and formation of nuclei, and the diffusion of the precursors on the substrate can be enhanced by the tunable kinetic energy provided by background pressure and deposition distance.[24–27]

Similarly, in these experiments, KrF-laser ablation of the GaSe target in vacuum (≈10^{-6} Torr) resulted in a typical ablation plume with a leading edge velocity of 2.2 cm μs^{-1}, corresponding to a maximum kinetic energy (Ga ions) of 175 eV (Figure S3 in Supporting Information). Deposition of GaSe under vacuum conditions resulted in the formation of thin films similar to conventional laser-deposited metal oxides. However, we found that the formation of 2D GaSe nanosheets required significant confinement and slowing of the plume by the Ar background gas (Figure S4 in Supporting Information), with a background gas pressure of ≈1 Torr a the target-to-substrate distance of 5 cm—typical conditions for the formation of ultrasmall nanoparticles in the plume.[25] Figure 1b,c shows the ICCD images of the plume evolution and R-t plot (R = target to substrate distance, and t = time) of the leading edge of the plume in an Ar background pressure of 1 Torr and 600 °C substrate temperature. A phenomenological $a = -\alpha v^2$ drag model, where $v = \frac{v_0}{1+\alpha v_0 t}; R = \alpha^{-1}\ln(1+\alpha v_0 t)$ is utilized to fit the curve.[27] The kinetic energies of the Ga and Se atoms at the surface of the substrate (placed 5 cm away from the target) significantly reduces to 1.1 and 1.3 eV, respectively. Higher background gas pressures (>5 Torr) resulted in the formation of large cluster aggregates that were deleterious to the formation of nanosheets. Time resolved ICCD images of the propagation and dynamics of the plume at different background pressures are provided (Figure S3 in Supporting Information).

At a given pressure and laser fluence, the precise control over deposition rate readily afforded by pulsed laser deposition was found to be advantageous in tuning growth morphology, as compared to chemical vapor deposition from chemically-reacted evaporation, where material flux is often very difficult to control. A temperature window of 500–750 °C was found to result in the growth of GaSe nanosheets. Substrate temperatures below 500 °C resulted in the deposition of amorphous GaSe, and no deposition was observed for substrate temperatures greater than 750 °C. Both out-of-plane and in-plane growth of GaSe nanosheets were controllably synthesized by adjusting the deposition rate (via laser repetition rate) and surface diffusion rate (via substrate temperature) for constant laser fluence, as shown in **Figure 2**a,b. Lower substrate temperatures and higher laser repetition rates (e.g. 550 °C, 3 Hz) increase the material deposition rates and reduce the surface diffusion rates. Consequently, these deposition conditions result in the formation of GaSe nanosheets oriented out-of-plane. As shown in Figure 2a, the nanosheets have typical thicknesses of just a few nanometers, corresponding to just 4–10 GaSe layers. At higher temperatures and lower laser repetition rates (e.g., 600 °C, 1 Hz), in-plane nanosheet growth was preferred.

The crystal structure of GaSe nanosheets transferred onto TEM grids were characterized by the high resolution transmission electron microscopy (HRTEM) images and electron diffraction. The periodicity of the lattice fringes in the TEM images are consistent with closed pack structures of multi-layer GaSe flakes with d_{100} spacing and lattice constant a of 3.21Å and 3.7Å, respectively, as shown in Figure 2c,d. The distances were measured from a Fourier transform of the image and SAED patterns. This structure indicates that the stacking of the layers can be either δ- or ε- type, the only structures that are

Adv. Funct. Mater. 2014,
DOI: 10.1002/adfm.201401440

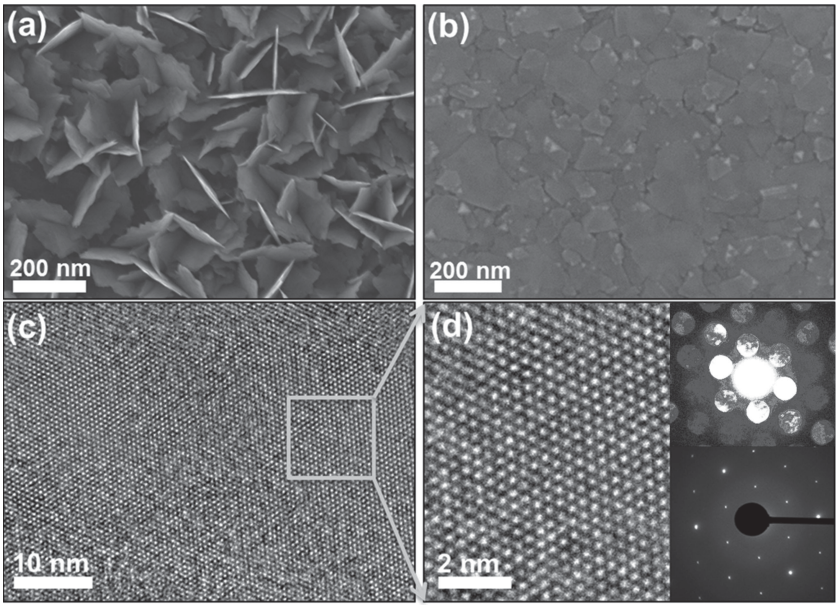

Figure 2. a) SEM image of out-of-plane GaSe nanosheets grown at substrate temperature of 550 °C and laser repetition rate of 3 Hz with typical thicknesses of just a few nanometers, corresponding to 4–10 GaSe layers. b) SEM image of in-plane GaSe nanosheets grown at substrate temperature of 600 °C and laser repetition rate of 1 Hz, while keeping the laser fluence at 1 J cm^{-2}. c,d) High-resolution TEM images, selected area diffraction patterns (bottom inset in d) and nano-beam diffraction patterns (top inset in d) of the nanosheet indicate hexagonal closed-pack GaSe with lattice constant *a* and *d* spacing of 3.7 and 3.21 Å, respectively.

consistent with the intensity inside the hexagons. The SAED pattern (bottom inset of Figure 2d) obtained from the [001] zone axis shows a single set of six-fold symmetry diffraction spots, indicating single crystalline nanosheets. Nanobeam (probe size <1 nm) diffraction (upper inset of Figure 2d) was also utilized to locally check the crystallinity of the few-layer GaSe nanosheets confirming the crystallinity and perfect stacking of these layers. Nanobeam diffraction is a type of convergent beam electron diffraction (CBED) where the Bragg reflections are widened to discs due to the variation of the incident beam angles. The intensity of the diffraction discs varies as one expects from dynamic diffraction of multilayer GaSe.

To understand the nucleation and growth process, GaSe nanosheets were deposited with a different number of laser pulses, and characterized with scanning electron microscopy (SEM) and atomic force microscopy (AFM), as shown in **Figure 3**. The correlation between the nanosheet flake size distributions and the number of laser pulses were also derived from the AFM images (Figure S5 in Supporting Information). At only ≈20 laser pulses into 1 Torr Ar at 600 °C (Figure S6 in Supporting Information), growth started with a large nucleation density (1–2 layers with lateral sizes ranging from 10–50 nm) with 40% substrate coverage. These initial layers on the SiO_2/Si substrate appeared to have random orientation relative to one another. However, as the number of pulses increased, the existing nuclei grew larger (100–200 nm) while forming new nuclei both on the substrate and on the top of the initial layers (Figure 3b). This continuous nucleation of new islands limits the size of the nanosheets until a continuous network is formed with a maximum surface roughness of ≈7 nm. Further deposition resulted in the formation of subsequent layers with the preferential filling of the layers near the substrate to decrease the surface roughness to a steady-state value of only a few nanometers corresponding to just 3–5 GaSe layers (Figure 3c). The film thickness can then be arbitrarily increased by depositing additional pulses. The number of the layers in Figure 3a–c were about 1–3, ≈10 and ≈20 layers, respectively.

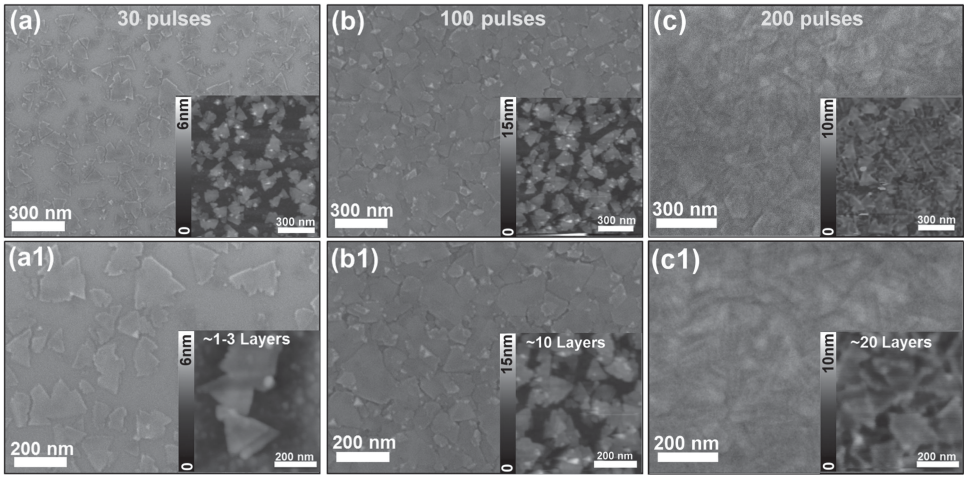

Figure 3. SEM and AFM (insets) images of GaSe nanosheets deposited onto SiO_2/Si substrate at 30 (a, a1), 100 (b, b1) and 200 (c, c1) laser pulses with substrate temperature of 600 °C, pressure of 1 Torr, and laser repetition rate of 1 Hz. The thickness of the deposited nanosheets networks was increased by increasing the number of pulses, resulting in the surface roughness of only few nanometers corresponding to just 3–5 GaSe layers.

This growth behavior at first appears similar to classic Volmer-Weber film growth, where numerous small nuclei grow driven by epitaxial strain with the substrate to coalesce into a thin film.[28,29] However, the observation of planar, triangular, crystalline nanosheets of GaSe that thicken with deposition time indicates that instead layer-by-layer-like growth is occurring within each island domain, with the observed high nucleation density of islands apparently resulting from the high-flux and cluster-rich conditions of the PLD plume in these experiments. In addition, the 2D layer-by-layer growth cannot be driven by epitaxy with the substrate for the SiO_2/Si substrates here, but can be attributed to the higher surface mobility of GaSe islands on as-formed GaSe layers. Each Se-Ga-Ga-Se layer of 4 atomic planes is held together with strong covalent bonding, however the adjacent layers can easily glide laterally due to weak, van der Waals bonding between layers at the Se-Se positions. Therefore, given sufficient mobility during deposition, small GaSe islands formed on a solid surface should preferentially assemble into 2D crystals in an apparent layer-by-layer growth mode, incorporating at the edges of the crystals due to strong edge-to-edge bonding there. In this context, the out-of-plane growth mode observed for higher incoming fluxes or lower temperatures can be explained by kinetic processes that alter in-plane 2D-island formation and restrict island mobility to disrupt this orderly "tiling" of 2D islands into lateral crystallites, resulting in the nucleation of out-of-plane edges. Because of the strong lateral bonding at these edges, GaSe layers can grow out-of-plane from these edges in directions which do not indicate a preferred crystallographic growth orientation. Further experimental and theoretical studies are under investigation to understand these detailed growth mechanisms.

Raman spectroscopy was also employed to characterize the crystalline quality and number of layers of the nanosheets. GaSe nanosheets deposited on the SiO_2/Si substrates were investigated by Raman spectroscopy and compared to bulk GaSe. As reported by others, GaSe has D_{3h} symmetry with 12 vibrational modes. Eight modes are in-plane (E′ and E″) and four are out-of-plane ($A_1'$and A_2'').[9,11,15] The Raman active modes are significantly thickness-dependent, and may be used to monitor the number of the layers. As shown in **Figure 4**, Raman spectra were collected from GaSe nanosheets with different thicknesses deposited on SiO_2/Si substrates and from the bulk GaSe target. The bulk crystal showed three intense peaks at 132 (A^1_{1g}), 211 (E^1_{2g}) and 308 cm^{-1} (A^2_{1g}) in addition to two weak peaks at 250 and 156 cm^{-1}. In contrast, the laser deposited 20-layers GaSe nanosheets showed a Raman spectrum similar to bulk. However, as the thickness of the nanosheets decreases, the intensity of the peaks at 133 and 208 cm^{-1} decrease significantly. Also, the A^2_{1g} peak at 308 cm^{-1} shifts to 303 cm^{-1} as the number of the layer decreases. A small peak also appears at 230 cm^{-1} in addition to a small shoulder at 250 cm^{-1} as the thickness approaches 1–3 layers. The variation of the Raman spectra vs. layer thickness correspond to what others have reported previously.[9,11,15]

Due to wide potential use of GaSe crystals in optoelectronics and optics, it is crucial to investigate the electrical transport and

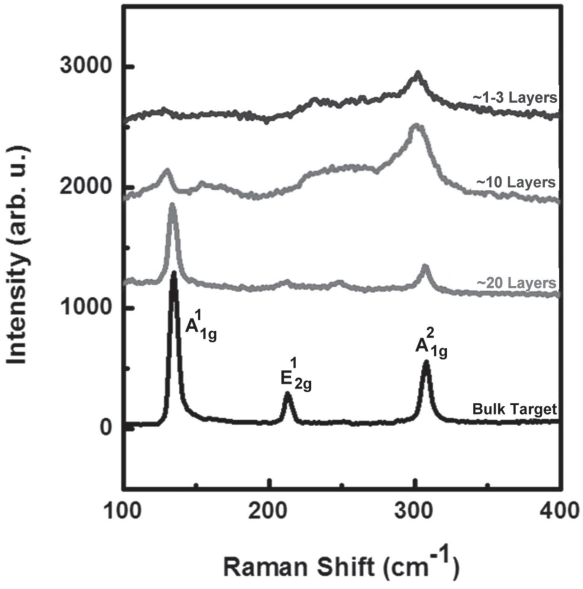

Figure 4. Raman spectra of GaSe obtained from samples shown in Figure 3(a), Figure 3(b), Figure 3(c) and bulk GaSe. A laser excitation source with a wavelength of 532 nm and 1mW of power was focused onto the GaSe nanosheets through a 100X objective for Raman measurement.

photoresponse of the present laser deposited nanosheets. **Figure 5** shows the electrical characteristics of a FET based on a ~20-layer GaSe nanosheet network. Transport is dominated by p-type behavior, and fitting the linear region of the drain current (I_D) and gate voltage (V_{GS}) (Figure 5a) gives the linear hole mobility μ_{lin} based on the relation in Equation (1).

$$I_D = (W/L)C_{ox}\mu_{lin}[V_{GS} - 1/2V_{DS} + V_T)]V_{DS}, \quad (1)$$

where W/L, C_{ox}, V_{DS}, V_T, are the width/length of the channel, specific capacitance of the gate oxide, drain to source voltage, and threshold voltage, respectively. The hole mobility and on/off ratio of the measured samples reached as high as 0.1 $cm^2V^{-1}s^{-1}$ and ~10^4, respectively. The highest mobility here (0.1 $cm^2V^{-1}s^{-1}$) is comparable to that obtained recently for mechanically exfoliated GaSe (0.6 $cm^2V^{-1}s^{-1}$).[10] Figure 5b shows the output characteristics that confirms typical saturation behavior. Here Au contacts were used as source and drain electrodes. The I_D–V_{DS} curves around the origin (Figure S7 in Supporting Information)

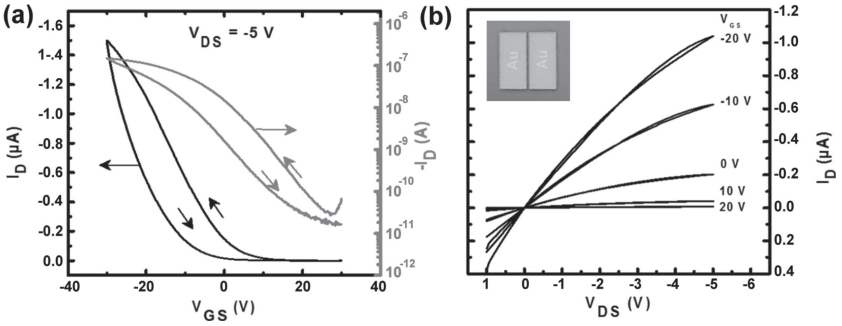

Figure 5. GaSe nanosheets field effect transistor electrical characteristics. (a) I_D–V_{GS} for device (inset in b) with width/length of 50/2000 μm, (b) I_D–V_{DS} output characteristics. The devices showed mobility as high as 0.1 $cm^2V^{-1}s^{-1}$ and on/off ratios of up to 10^4.

DOI: 10.1002/adfm.201401440

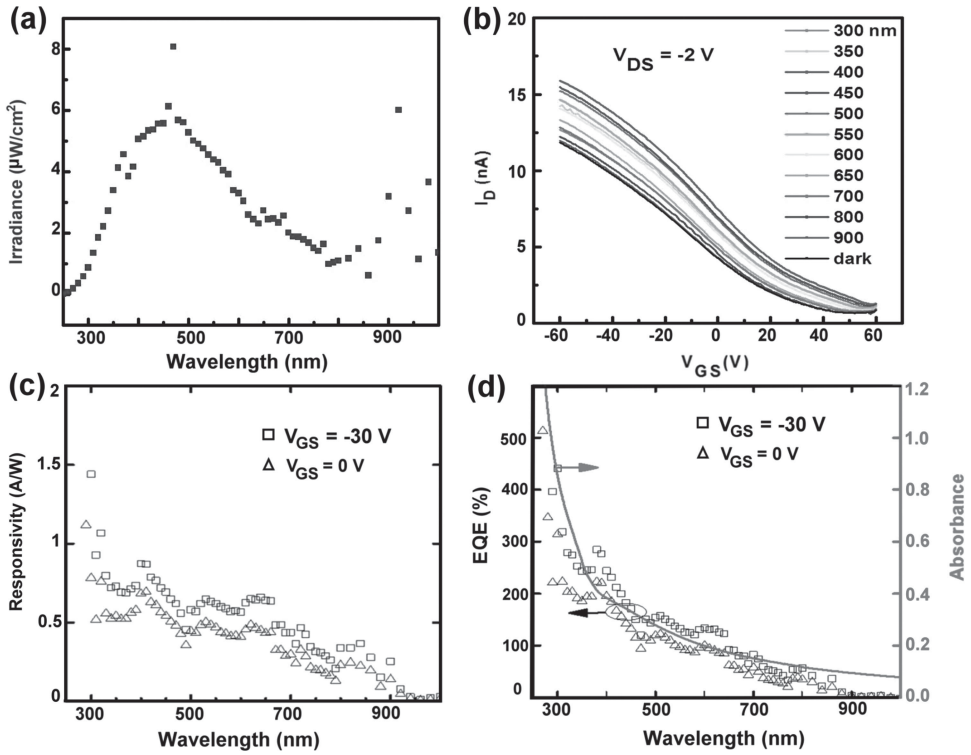

Figure 6. GaSe nanosheets photoresponse characteristics. a) Spectral irradiance of the light source measured at the sample position and used for responsivity measurements. b) I_D–V_{GS} characteristics for select wavelengths of incident monochromatic light. c) Spectral responsivities at $V_{GS} = -30$ (squares) and 0 V (triangles) of 20-layer GaSe nanosheet networks as a function of wavelength with increasing trend from 0 AW^{-1} at 1000 nm up to 1.4 AW^{-1} at 240 nm. d) EQE (corresponding to responsivities of 0–1.4 AW^{-1}) with comparison to absorbance of GaSe nanosheets on a fused silica substrate fabricated under the same conditions (red line).

show near linear and symmetrical dependences. It should also be mentioned that GaSe interfaces with various metals, including interacting (Cu, Al, Ni, In) and non-interacting (Au, Ag, Sn), have been previously reported showing no Fermi pinning effect for non-interacting metals such as gold.[30]

Figure 6 shows the optical characteristics GaSe nanosheet network. The spectral irradiance of the light source used for responsivity measurements and the I_D–V_{GS} curves as function of incident monochromatic light are shown in Figure 6a,b. I_D–V_{DS} output characteristics for dark and room light illumination conditions are also shown (Figure S8 in Supporting Information). The largest response is seen for 240 nm, the mobility (slope) does not vary significantly and only a shift in V_T (x-intercept) is observed. The spectral responsivity (Figure 6c) is measured and the external quantum efficiency (EQE) (Figure 6d) is given by Equation (2).

$$\mathrm{EQE} = R_\lambda hc / (e\lambda), \tag{2}$$

where R_λ is the spectral responsivity ($\Delta I/PA$) defined by the difference in current between light and dark ΔI and the incident light power density P on the FET channel area A, and h, c, e, and λ are Plank's constant, the speed of light, elementary charge, and wavelength of incident light, respectively. The general trend is an increase in photoresponse towards UV light with a tail towards the infrared. Consequently, spectral responsivities (R_λ) range from 0.4–1.4 AW^{-1} which are comparable to responsivities reported for exfoliated 2D GaSe (2.8 AW^{-1}, illuminated with 254 nm),[9] and higher than epitaxial (0.6 AW^{-1}, illuminated with white light)[31] and vapor-phase grown GaSe sheets (17 mAW^{-1}, illuminated with 405 nm).[15] Utilizing the values obtained for spectral responsivities and Equation 1, the corresponding EQE ranged from 100% at 700 nm to 600% at 240 nm.

To elucidate the origin of the photoresponse, we compared the EQE of FETs to the optical absorption of laser-deposited GaSe layers on fused silica substrates (Figure 5d). A general trend of increasing absorption towards the UV is apparent as expected for GaSe. Features at ~3.6 eV and ~4.9 eV are seen for all thicknesses and attribute these to the E_1 and E_3 electronic transitions.[32]

The large spectral responsivity (above unity), shift of V_T due to incident light, response below the bandgap (2.1 eV) and long photoresponse times (Figure S9 in Supporting Information) suggests that midgap states are responsible for the observed photocurrent, where absorbed photons interact with these states. These states could be due to a number of factors including dangling bonds at the edge of the nanosheets or interactions with the gate oxide or environment. Further investigation is needed to determine the origin of these states.

3. Conclusion

In conclusion, we report the direct growth of GaSe nanosheet networks on insulating substrates by pulsed laser deposition.

High (1 Torr) Ar background gas pressures were required for the preservation of film stoichiometry from the GaSe bulk target, with a maximum of ≈1 eV kinetic energy of plume atoms at the substrate. Interconnected few-layer crystalline GaSe nanosheet networks with controlled thicknesses could be rapidly synthesized with good uniformity over 1.5 cm^2 areas, with out-of-plane or in-plane orientation determined by the substrate temperature and laser repetition rate, and thickness determined by laser shot number. SEM, AFM, TEM and Raman spectroscopy confirmed the thickness and quality of the synthesized GaSe. Electrical transport measurements of GaSe-based FETs indicated a maximum mobility of 0.1 $cm^2V^{-1}s^{-1}$ and on/off ratios of 10^4. The optoelectronic properties showed photoresponsivity and external quantum efficiency ranging from 0.4 AW^{-1} and 100% at 700 nm, to 1.4 AW^{-1} and 600% at 240 nm, respectively. These high photoresponsivities appear to be related to midgap states which likely arise from the numerous grain boundaries in the polycrystalline nanosheet networks. Pulsed laser deposition therefore appears promising as it provides a versatile and rapid approach to stoichiometrically transfer and deposit functional networks of 2D nanosheets with digital thickness control and substrate-scale uniformity for a variety of applications.

4. Experimental Section

Crystal Synthesis: To prepare the laser ablation target, 29 g (total) of Ga (Alfa Aesar, 99.9999%) and Se (Alfa Aesar, 99.999%) shot was placed inside a 19 mm ID fused silica ampoule, and sealed under high vacuum. The ampoule was heated slowly to 980 °C, and held at this temperature for six hours. Twice during the soak at 980 °C, the furnace was opened and the ampoule shook gently to eliminate bubbles trapped between the melt and the wall of the ampoule. After six hours, the furnace was turned off and allowed to cool to room temperature. The resulting boule was ruby colored stoichiometric GaSe, and appeared to be composed of many large flakes each several mm in size (Figure S1, S2 in Supporting Information).

Pulsed Laser Deposition: A 2.5-cm-diam stainless steel heater (HeatWave Labs, Inc.) was placed d = 5cm away and parallel to a 1.9-cm-diam GaSe bulk crystalline in a cylindrical chamber (50 cm inner diameter, 36 cm tall). The GaSe target was ablated by imaging a rectangular aperture illuminated by an excimer laser (KrF 248 nm, 20 ns full width at half maximum (FWHM)) at 5:1 reduction) onto the target. The resultant spot size and energy density were 2×5 mm^2 and 1 Jcm^{-2}, respectively. The target was irradiated at 30° angle of incidence with repetition rates of 1–5 Hz. Gas pressure was controlled in a 0.2–10 Torr pressure range with a mass flow controller (Ar 99.995%, 0–500 sccm) and downstream throttle valve controller. The vacuum chamber was pumped to 1×10^{-6} Torr prior to deposition. The heater was controlled by an integrated thermocouple to ± 2 °C. The plume imaging was performed with an ICCD camera system (Princeton Instruments, PI-MAX) with gating above 5 ns. The detector was positioned 46 cm away from the plume center, outside the chamber, looking at the plume through a Suprasil window. Exposures time and f-stop were varied from 5 ns–5 ms, and 32–4.5, respectively.

Characterization of GaSe Nanosheet Networks: SEM (Zeiss Merlin VP SEM microscope system), HRTEM images and electron diffraction patterns (Zeiss Libra 200 MC transmission electron microscope, with accelerating voltage at 200kV), AFM (Bruker Dimension Icon), and Raman spectroscopy (532 nm excitation source with 1mW of power focused onto the samples through a 100X objective lens) were used to characterize the samples. GaSe nanosheets were released from the substrate surface by etching the oxide layer using buffer oxide etchant (BOE) and collecting them on TEM grids (SPI, 200 mesh Lacey carbon).

Electrical and Photoresponse Measurements: GaSe nanosheets were grown directly on highly doped p-type silicon substrates having a 300 nm thermal oxide. Back-gated field effect transistors (FETs) with a channel width/length of 2000/50 μm were fabricated by thermally depositing 50 nm thick gold electrodes onto the nanosheets through a contact mask. The FETs were characterized with a Keithley 4200 Semiconductor Characterization System, and in cases where spectral responsivity was required, these measurements were performed in a light tight box. The light source used for the responsivity measurements was comprised of a 300W Oriel Xe lamp in series with a 1/8m Oriel Cornerstone 130 monochromator, equipped with a cutoff filter to remove the light from the second order of the grating. The slits of the monochromator were adjusted to achieve a pass band of 10 nm FWHM, and the spectral irradiance of the output at the sample position was measured by a NIST-traceable photodetector (918D-UV-OD3R), and a Newport 1936-C/R Optical Power and Energy Meter. The output beam (2 mm diam) covered the entire channel area of the device photoresponse measurements.

Supporting Information

Supporting Information is available from the Wiley Online Library or from the author.

Acknowledgements

Synthesis science was sponsored by the Materials Sciences and Engineering Division, Office of Basic Energy Sciences, US Department of Energy. Characterization science was performed at the Center for Nanophase Materials Sciences, which is sponsored at Oak Ridge National Laboratory by the Scientific User Facilities Division, Office of Basic Energy Sciences, US Department of Energy. R.G. acknowledges support from the Advanced Manufacturing Office, Office of Energy Efficiency and Renewable Energy, US Department of Energy (photoresponsivity measurements).

Received: May 3, 2014
Revised: June 11, 2014
Published online:

[1] C. Berger, Z. Song, X. Li, X. Wu, N. Brown, C. Naud, D. Mayou, T. Li, J. Hass, A. N. Marchenkov, E. H. Conrad, P. N. First, W. A. de Heer, *Science* **2006**, *312*, 1191.
[2] K. S. Novoselov, A. K. Geim, S. V. Morozov, D. Jiang, Y. Zhang, S. V. Dubonos, I. V. Grigorieva, A. A. Firsov, *Science* **2004**, *306*, 666.
[3] A. K. Geim, K. S. Novoselov, *Nat. Mater.* **2007**, *6*, 183.
[4] K. S. Novoselov, D. Jiang, F. Schedin, T. J. Booth, V. V. Khotkevich, S. V. Morozov, A. K. Geim, *Proc. Natl. Acad. Sci. USA* **2005**, *102*, 10451.
[5] J. N. Coleman, M. Lotya, A. O'Neill, S. D. Bergin, P. J. King, U. Khan, K. Young, A. Gaucher, S. De, R. J. Smith, I. V. Shvets, S. K. Arora, G. Stanton, H. Y. Kim, K. Lee, G. T. Kim, G. S. Duesberg, T. Hallam, J. J. Boland, J. J. Wang, J. F. Donegan, J. C. Grunlan, G. Moriarty, A. Shmeliov, R. J. Nicholls, J. M. Perkins, E. M. Grieveson, K. Theuwissen, D. W. McComb, P. D. Nellist, V. Nicolosi, *Science* **2011**, *331*, 568.
[6] J-G. Song, J. Park, W. Lee, T. Choi, H. Jung, C. W. Lee, S-H. Hwang, J. M. Myoung, J-H. Jung, S-H. Kim, C. Lansalot-Matras, H. Kim, *ACS Nano* **2013**, *7*, 111333.
[7] C. Lee, Q. Li, W. Kalb, X. Z. Liu, H. Berger, R. W. Carpick, J. Hone, *Science* **2010**, *328*, 76.

[8] D. Teweldebrhan, V. Goyal, A. A. Balandin, *Nano Lett.* **2010**, *10*, 1209.
[9] P. A. Hu, Z. Wen, L. Wang, K. Xiao, *ACS Nano* **2012**, *6*, 5988.
[10] D. J. Late, B. Liu, J. Luo, A. Yan, H. S. Matte, M. Grayson, C. N. Rao, V. P. Dravid, *Adv. Mater.* **2012**, *24*, 3549.
[11] J. L. Dattatray, B. Liu, H. S. S. Ramakrishna Matte, C. N. R. Rao, V. P. Dravid, *Adv. Funct. Mater.* **2012**, *22*, 1894.
[12] Y. Shi, W. Zhou, A-Y. Lu, W. Fang, Y-H. Lee, A. L. Hsu, S. M. Kim, K. K. Kim, H. Y. Yang, L.-J. Li, J-C. Idrobo, J. Kong, *Nano Lett.* **2012**, *12*, 2784.
[13] D. P. Duttaa, G. Sharmab, A. K. Tyagia, S. K. Kulshreshthaa, *Mat. Sci. Eng. B* **2007**, *138*, 60.
[14] L. Song, L. Ci, H. Lu, P. B. Sorokin, C. Jin, J. Ni, A. G. Kvashnin, D. G. Kvashnin, J. Lou, B. I. Yakobson, P. M. Ajayan, *Nano Lett.* **2010**, *10*, 3209.
[15] S. Lei, L. Ge, Z. Liu, S. Najmaei, G. Shi, G. You, J. Lou, R. Vajtai, P. M. Ajayan, *Nano Lett.* **2013**, *13*, 2777.
[16] Z. Y. Yin, H. Li, H. Li, L. Jiang, Y. Shi, Y. Sun, G. Lu, Q. Zhang, X. Chen, H. Zhang, *ACS Nano* **2012**, *6*, 74.
[17] O. Lopez-Sanchez, D. Lembke, M. Kayci, A. Radenovic, A. Kis, *Nat. Nanotechnol.* **2013**, *8*, 497.
[18] G. Cunningham, U. Khan, C. Backes, D. Hanlon, D. McCloskey, J. Donegan, J. N. Coleman, *J. Mater. Chem. C* **2013**, *1*, 6899.
[19] A. Kuhn, A. Chevy, R. Chevalier, *Phys. Stat. Sol.* **1975**, *31*, 469.
[20] C. W. Chen, Y. K. Hsu, J. Y. Huang, C. S. Chang, J. Y. Zhang, C. L. Pan, *Opt. Express.* **2006**, *14*, 10636.
[21] L. Leontie, I. Evtodiev, V. Nedeff, M. Stamate, M. Caraman, *Appl. Phys. Lett.* **2009**, *94*, 071903.
[22] W. C. Chu, S. A. Ku, H. J. Wang, C. W. Luo, Y. M. Andreev, G. Lanskii, T. Kobayashi, *Opt. Lett.* **2012**, *37*, 945.
[23] W. Shi, M. Leigh, J. Zong, S. Jiang, *Opt. Lett.* **2007**, *32*, 949.
[24] D. H. Lowndes, D. B. Geohegan, A. A. Puretzky, D. P. Norton, C. M. Rouleau, *Science* **1996**, *273*, 898.
[25] D. B. Geohegan, A. Puretzky, G. Duscher, S. J. Pennycook, *App. Phys. Lett.* **1998**, *72*, 2987.
[26] D. B. Geohegan, A. Puretzky, *App. Phys. Lett.* **1999**, *74*, 3788.
[27] D. B. Geohegan, *Eximer Lasers: The Tools, Fundamental Processes and Applications* Kluwer Academic Publisher, The Netherlands, **1994**, 165.
[28] C. Polop, C. Rosiepen, S. Bleikamp, R. Drese, J. Mayer, A. Dimyati, T. Michely, *New J. Phys.* **2007**, *9*, 74.
[29] S. Franssila, *Introduction to Microfabrication: Thin-Film Growth and Structure* John Wiley and Sons, Chichester, UK **2004**, 73.
[30] G. J. Hughes, A. McKinley, R. H. Williams, I. T. McGovern, *J. Phys. C: Solid State Phys.* **1982**, *15*, 159.
[31] Y. Zhou, Y. Nie, Y. Liu, K. Yan, J. Hong, C. Jin, Y. Zhou, J. Yin, Z. Liu, H. Peng, *ACS Nano* **2014**, *8*, 1485.
[32] S. Adachi, Y. Shindo, *J. Appl. Phys.* **1992**, *71*, 428.